

# Percolation-based precursors of transitions in spatially extended systems

Víctor Rodríguez-Méndez, Víctor M. Eguíluz, Emilio Hernández-García, and José J. Ramasco  
*IFISC (CSIC-UIB), Instituto de Física Interdisciplinar y Sistemas Complejos,  
 Campus Universitat de les Illes Balears, E-07122 Palma de Mallorca, Spain.*

(Dated: May 23, 2022)

Abrupt transitions are ubiquitous in the dynamics of complex systems. Finding early indicators of their arrival, precursors, is fundamental in many areas of science such as ecology, electrical engineering, physiology or climate. However, obtaining warnings of an approaching transition well in advance remains an elusive task. Here we show that a functional network, constructed from spatial correlations of the system's time series, experiences a percolation transition way before the actual system reaches a bifurcation point due to the collective phenomena leading to the global change. Concepts from percolation theory are then used to introduce early warning precursors that anticipate the system's tipping point. We illustrate the generality and versatility of our percolation-based framework with model systems experiencing different types of bifurcations and with Sea Surface Temperature time series associated to El Niño phenomenon.

Abrupt transitions are ubiquitous in the dynamics of complex systems. Finding early indicators of their arrival, precursors, is fundamental in many areas of science such as ecology[1], electrical engineering [2], physiology[3] or climate [4–6]. However, obtaining warnings of an approaching transition well in advance remains an elusive task. Here we show that a functional network, constructed from spatial correlations of the system's time series[7–9], experiences a percolation transition way before the actual system reaches a bifurcation point due to the collective phenomena leading to the global change. Concepts from percolation theory[11, 12] are then used to introduce early warning precursors that anticipate the system's tipping point. We illustrate the generality and versatility of our percolation-based framework with model systems experiencing different types of bifurcations and with Sea Surface Temperature time series associated to El Niño phenomenon.

Management of complex systems requires the detection with sufficient anticipation of approaching critical or tipping points. Early-warning signals have been introduced and tested in recent works [13–15], including experimental verification in living and environmental systems [14, 16, 17]. These methods rely on the loss of resilience occurring generically when the system approaches most (although not all) types of bifurcation points[5, 15, 18]. Recovery rates from perturbation become small, leading to critical slowing down of the dynamics, increased memory and long temporal autocorrelations, and to growth of the temporal variance [5, 15, 18]. From a dynamical viewpoint, these phenomena appear when the eigenvalue of the Jacobian matrix describing the rate of relaxation towards the attractor approaches zero close to bifurcation points. In many cases, particularly when different spatial parts of the system are coupled by diffusion-like processes, the increase in temporal correlation is accompanied by the growth of spatial correlations [19–21]. This, with the associated increase in spatial variance and response functions, is actually a standard method to characterize phase transitions in thermodynamic physical sys-

tems.

The consideration of spatial correlations has led to a novel perspective for finding transition precursors through the use of correlation or functional networks [7, 8]. These networks are built measuring the correlation among all pairs of spatial units composing the system and keeping the most significant ones as link weights. Several network-based precursors have been proposed. Specifically the values of the degree (number of connections per node), assortativity (degree-degree correlations), clustering (average density of network triangles) and kurtosis raise when approaching a tipping point[22–24].

Here we show an important additional property of the functional networks: As internal correlations increase, networks evolve from a low to a high connectivity state and, *before* reaching its maximum link density at the bifurcation point, a percolation-like transition occurs in the network topology. Concepts from graph percolation theory [11, 12] can thus be imported to characterize this transition. Importantly, metrics can be defined that act as early warnings for this percolation transition, which itself is a precursor of the dynamic transition.

As a first example, we consider a lake eutrophication (LE) model[28] that suffers a paradigmatic abrupt transition associated to a saddle-node (SN) bifurcation (see Methods). Similar results are obtained for other models with different types of transitions (see below and Supplementary Information). The LE model describes a transition between two contrasted states for the phosphorous concentration  $\psi(\mathbf{x}, t)$  in a lake: low concentrations leading to clear water, and excess of phosphates leading to turbid water. The control parameter  $p$  is the nutrient input rate into the lake and the transition point  $p_d$  (see Fig. 1) identifies the value beyond which a switch occurs from the clear to the turbid state. A raise of the spatial variance of the field  $\psi$  (used in [5, 15, 18] as transition indicator) when the system approaches  $p_d$  can be observed in Fig. 1b. We constructed functional networks by assigning links between locations among which spatial correlations (as measured by Pearson correlation, see

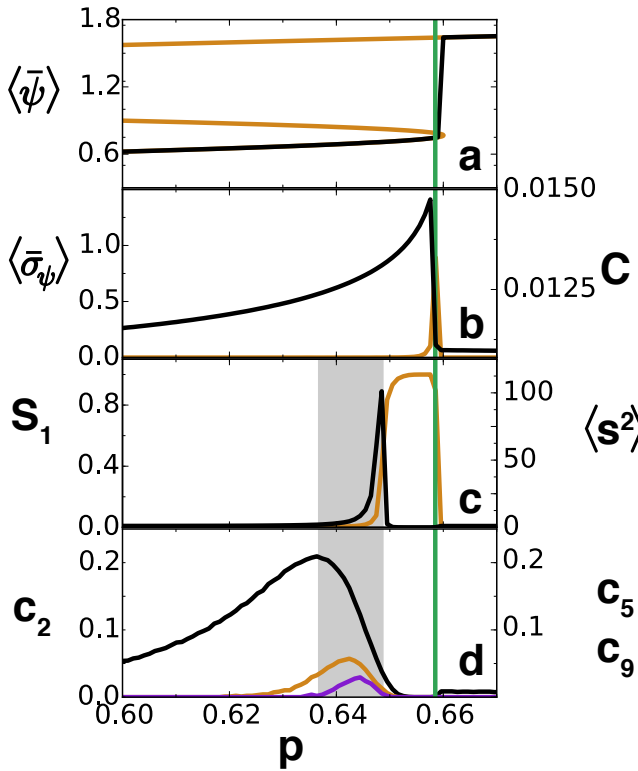


FIG. 1: **Transition precursors for the LE model, equation (1).** In **a**, the steady homogeneous phosphorous concentration  $\psi$  (orange) and the numerically obtained spatial average (black, further averaged over  $T = 1000$  temporal snapshots for each value of  $p$ ) as a function of the control parameter  $p$  which is slowly increased from low to high values. In **b**,  $\langle \bar{\sigma}_\psi \rangle$ , the spatial standard deviation (black) of  $\psi$  averaged over  $T = 1000$  temporal snapshots. In orange the clustering of the functional network built with threshold  $\gamma = 0.21$ . In **c**, the relative size of the giant component,  $S_1$  (orange), and the average size of the leftover clusters ( $\langle s^2 \rangle$ , black). In **d**, the probabilities  $c_2$  (black),  $c_5$  (orange), and  $c_9$  (purple) are shown. In all the panels, the vertical green line marks the position of the observed abrupt transition ( $p_d = 0.658$ ). The grey area indicates the anticipation in parameter space gained by using the peak of  $c_2$  as precursor of the percolation transition. All curves have been further averaged over 100 realizations of the random noise and initial conditions.

Methods) are larger than a threshold  $\gamma$ . The correlation increase leads to a growth of the link density in the vicinity of the critical point as indicated by the precursors proposed in [22–24]. In fact, the clustering showed in Fig. 1a (orange) has a peak at the dynamical transition. But there is also a percolation transition, and to capture it we studied how the size of the giant component,  $S_1$ , and the average size of the leftover clusters ( $\langle s^2 \rangle$ , see Methods) change with  $p$  (see Fig. 1c). Note that  $\langle s^2 \rangle$  has a peak at  $p = 0.648$ , which identifies the occurrence of percolation in the network, way before the SN transition has happened, and thus it may be used as a signal that a dynamical transition is coming. The distance in the

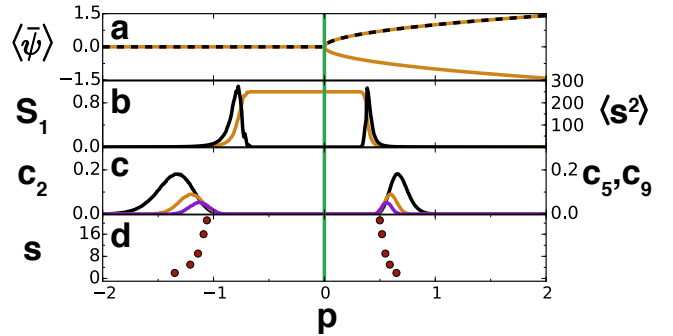


FIG. 2: **Peaks of  $c_s$  as transition precursors in the GL model.** The GL model has a continuous transition at the critical value  $p_d = 0$  marked by the green line. In **a**, the theoretical (yellow) and the numerically obtained (black dash line, further averaged over  $T = 1000$  temporal snapshots) homogeneous value of the field  $\psi$  are shown. Functional networks were built using a threshold of  $\gamma = 0.25$ .  $S_1$  (orange) and  $\langle s^2 \rangle$  (black) are displayed in the panel **b**. Panel **c** shows  $c_2$  (black),  $c_5$  (orange), and  $c_9$  (purple). In **d**, the circles indicate the values of  $p$ ,  $p_s$  with  $s = 2, 5, 9, 16$  and  $21$ , for which  $c_s$  attains its respective maximum.

parameter space between that signal and the transition depends on which threshold is used to build the network, but there is an optimal value (see below).

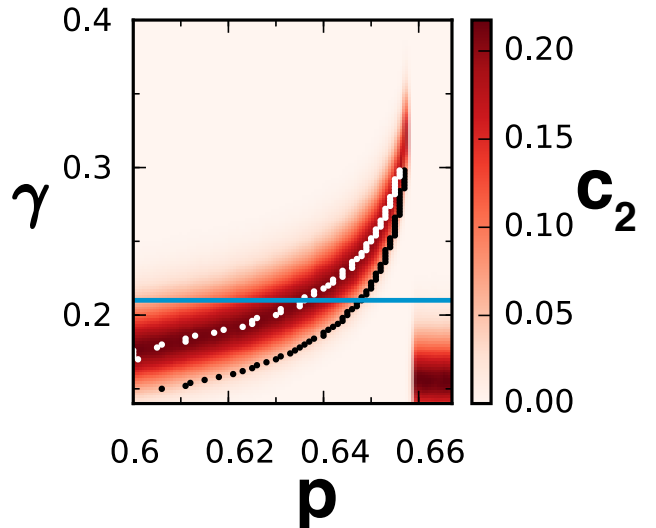


FIG. 3: **Role of the correlation threshold  $\gamma$ .**  $c_2$  values, as given by the color bar, as a function of the control parameter  $p$  and the threshold  $\gamma$  used to build the functional network for the LE model. The white dots give the locations of the  $c_2$  maxima, while the black dots mark the maxima of  $\langle s^2 \rangle$  (percolation transition). The dynamical sudden jump occurs at  $p_d = 0.658$ . The horizontal blue line identifies the value of  $\gamma = 0.21$  used in Fig. 1. Similar plots for other models are in Supplementary Information.

The percolation transition is not, however, the best precursor. Better anticipation can be obtained by ex-

plotting a phenomenon observed for percolation in random graphs. In such graphs, as new links are being added at random, percolation occurs when the mean degree  $\langle k \rangle$  equals one. Before this, the probability that a randomly chosen node belongs to a small component of size  $s$  is given by[12]  $c_s = e^{-s\langle k \rangle} (s\langle k \rangle)^{s-1}/s!$ . This probability has a maximum when the mean degree is  $\langle k \rangle = k_s = \frac{s-1}{s}$ . The succession  $\{k_s\}$  of location of maxima of  $c_s$  converges to the percolation point  $k_\infty = 1$  for increasing component size  $s$ , but for low  $s$  these maxima could be quite far from the percolation point, anticipating it. We check that this early warning character of  $c_s$  is also present in our non-random functional networks. The probabilities  $c_2$ ,  $c_5$  and  $c_9$  for the networks built from the LE system are shown in Fig. 1d. Their maxima clearly anticipate the percolation transition signaled by  $S_1$  and  $\langle s^2 \rangle$ , which gives itself an early warning of the SN bifurcation. The peak in  $c_2$  appears at  $p_2 = 0.635$ , anticipating  $p_d$  more than twice as early as the percolation transition.

To prove the generality of the precursors we analyze a different system, the Ginzburg-Landau equation, which is a paradigmatic model experiencing a continuous transition (see Methods). Figure (2a) shows averages of the spatial mean field  $\bar{\psi}$ . Here correlations continuously build-up when increasing  $p$  towards the critical point at  $p_d = 0$  and, unlike the previous discontinuous transition, continuously decrease after crossing it. Therefore, there are now two percolation transitions in the functional networks: one at each side of  $p_d$ , as seen by the indicators  $S_1$  and  $\langle s^2 \rangle$  in Fig. 2b. Figure 2c depicts the probabilities  $c_2$ ,  $c_5$  and  $c_9$ , giving a clear warning further away from  $p_d$ . Figure 2d displays the values  $p_s$  corresponding to the maxima in  $c_s$ . There are two successions of peaks converging to the percolation transitions occurring before and after the bifurcation.

Building functional networks involves to fix the correlation threshold  $\gamma$  above which two elements are considered as linked. Figure 3 shows (for the LE model; results for other models are in Supplementary Information) how the percolation transition and the values of  $c_2$  depend on both  $p$  and  $\gamma$ . If  $\gamma$  is very high, the network is never connected and there is no signal. Similarly, if  $\gamma$  is very low the network is always fully connected and there is no hint of the bifurcation. However, as shown in the figure there is a range of values of  $\gamma$  where the percolation transition and its associated early warning signals appear. For a fixed value of  $\gamma$  the peak of  $c_2$  (white dots) always occurs earlier than the percolation transition (black dots). As  $\gamma$  decreases, the peak of  $c_2$  occurs at earlier values of  $p$ . The curve of  $c_2$ , however, widens and the resolution in the location of the peak gets poorer. The lowest (optimal) value of  $\gamma$  at which the peak can be distinguished marks thus the earliest warning signal that can be obtained for the bifurcation. The behavior exemplified in Fig. 3 is common to several types of transitions, as shown in the Supplementary Information.

To test the behavior of our precursors in a real situation, we analyze sea surface temperature data from

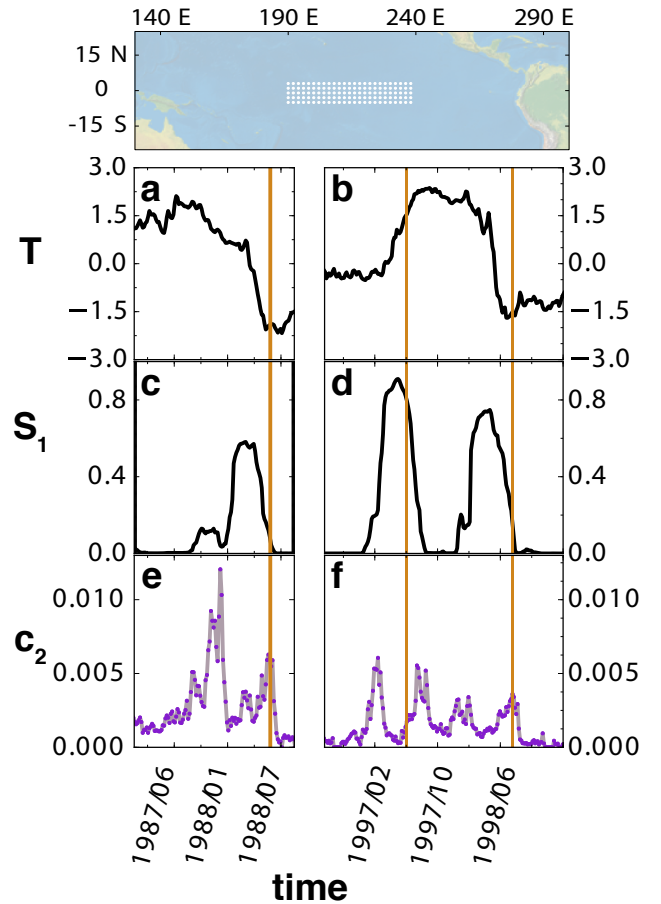


FIG. 4: **Application to El Niño phenomenon.** The upper panel shows a map of the area over which the mean Sea Surface Temperature  $T$  is monitored in the NINO3.4. Points denote locations used here as nodes in a functional network. Three events, two La Niña (cold) and one El Niño (warm), are shown in the time axis of panels **a** to **f**. Conventional starting dates of the events are marked by vertical orange lines. In **a** and **b**, the sea surface temperature  $T$  as a function of time. A functional network is constructed from correlations at  $\gamma = 1 - \varepsilon$  with  $\varepsilon = 8 \times 10^{-5}$ . The size of the giant component  $S_1$  is shown in panels **c** and **d**, showing percolating phases at a plateau, flanked by two percolation transitions, which occurs before each of the events. Panels **e** and **f** show  $c_2$  in the same time frame. Maxima in  $c_2$  flank both sides of the percolation plateaux, in a manner similar to the Ginzburg-Landau case shown in Fig. 2.

the region of the Pacific used to compute the NINO3.4 index[25]. El Niño-Southern Oscillation[26, 27] is the dominant variability mode in present-day climate, characterized by rather irregular (with average period of about 4 years) warm (El Niño) and cold (La Niña) episodes departing from the long-term mean temperature in the equatorial Pacific. These oscillations are related to the presence of a Hopf bifurcation in the coupled atmosphere-ocean system[26, 27]. The bifurcation can be crossed or just approached, being then the oscillation excited by noise. In both cases there should be a build-up

of correlations that would become visible in functional networks constructed from temperature time series. In this case there is no control parameter to fix, but rather the equatorial Pacific evolves in time, coupled to the seasonal cycle, leading to changing spatial correlations. We construct functional networks from time windows of the time series from different locations (see Fig. 4) and analyze them with the methods developed above.

We have focused on two different periods: 1987–1989, during which a strong La Niña occurred, and 1996–1998, featuring one El Niño-La Niña pair. Modifying  $\gamma$ , it is possible to find a range of values in which a percolation transition is observed. Fixing  $\gamma$  where the signal-to-noise ratio is stronger, a pair of percolation transitions is clearly seen enclosing a percolated phase with a large value of  $S_1$  for each of the events. The indicator  $c_2$  has maxima before and after the two percolation transitions associated to each event. The full picture is strongly reminiscent of the situation found with the Ginzburg-Landau model in Fig. 3, characteristic of a continuous transition.

We have shown that consideration of the percolation transition in functional networks constructed from spatial correlations in extended systems provides powerful anticipatory tools for their dynamical regime shifts. Precursors of the percolation transition itself, such as the probabilities  $c_s$  for random nodes to belong to small clusters, add extra anticipatory range. We note that  $\gamma$  and  $s$  are methodological parameters, so that they can be explored even when far from the dynamical transition. Then plots similar to partial versions of Figs. 2d or 3 can give a hint on the distance to the approaching transition. The tools presented here work in a variety of transition types, provided correlations increase when approaching them, and are useful even in cases, such as El Niño events, where very little information on the underlying dynamics is available. Thus we expect they will become instrumental in the monitoring and management of complex systems.

## METHODS

We have considered two dynamical models with different bifurcations and also the Sea Surface Temperature time series from the Pacific Ocean. Results for a third model (the Lorenz'96 model) are included in the Supplementary Information.

The first model, the LE model, is representative of systems experiencing a SN bifurcation. It is a spatial version of a description of phosphorous recycling in a lake [28]. The state of the system is given by the two-dimensional field  $\psi(\mathbf{x}, t)$  representing the amount of phosphorous in the lake, evolving according to

$$\frac{\partial\psi(\mathbf{x}, t)}{\partial t} = p - b\psi(\mathbf{x}, t) + rf(\psi) + \epsilon\nabla^2\psi(\mathbf{x}, t) + \eta(\mathbf{x}, t). \quad (1)$$

$f(\psi) = \psi^8/(\psi^8 + 1)$  is a nonlinear response of the lake sediments to phosphorous,  $p$  is the nutrient rate input,

taken here as the control parameter.  $\epsilon$  is the strength of diffusive spatial coupling, and  $\eta$  represents an additive stochastic perturbation uncorrelated in space and time. We take  $b = r = 1$  and  $\epsilon = 1.2$ . Space is discretized as a square lattice of  $N = 70 \times 70 = 4900$  grid points separated by  $dx = 1$ . These will be the nodes of the functional network. The Laplacian is discretized with the simplest finite differences scheme and the deterministic terms in equation (1) are integrated with a 4th order Runge-Kutta method of time step  $dt = 0.05$  after which the  $\eta$  term is implemented by adding an independent random number uniform in  $[-a, a]$  to each lattice site (we use  $a = 0.125$ ). We approach from the left the SN bifurcation occurring at  $p = p_{SN} = 0.660$ , above which the clear-water low-phosphorous state existing for  $p < p_{SN}$  ceases to exist and the lake jumps to an eutrophicated high-phosphorous state. The stochastic perturbation makes the jump to occur at a value of  $p$ ,  $p_d$ , slightly below the SN value. On average (see Fig. 1), we find  $p_d \approx 0.658$ . This value is sufficiently close to  $p_{SN}$  as to display the enhancement of correlations and slowing down which are at the basis of our method and of other early-warning methodologies. In this paper we have only displayed results obtained when slowly increasing the control parameter  $p$ . When decreasing  $p$  from higher values hysteresis occurs and a different SN bifurcation is encountered at a lower  $p'_d \approx 0.389$ . The sequence of precursors encountered when approaching this lower transition point is similar to the one shown here.

As a second model, we consider the time-dependent Ginzburg-Landau equation[29] or model A describing, for example, transitions in anisotropic ferromagnets. We study the one-dimensional version for the magnetization  $\psi(x, t)$ :

$$\frac{\partial\psi(x, t)}{\partial t} = p\psi(x, t) - \psi(x, t)^3 + \epsilon\nabla^2\psi(x, t) + \eta(x, t). \quad (2)$$

As before,  $\epsilon$  is diffusive coupling and  $\eta$  is an additive uncorrelated noise uniform in  $[-a, a]$ . We discretize equation (2) into  $N = 5000$  nodes, and take  $\epsilon = 1.5$ ,  $a = 0.01$ . The integration parameters  $dt$  and  $dx$  are as before. A continuous transition from zero magnetization occurs when increasing the control parameter  $p$  above  $p_d = 0$ .

For the climatic data analysis, Sea Surface Temperatures were obtained from the ERA-interim reanalysis of the European Centre for Medium-Range Weather Forecasts[30], with daily temporal resolution and a spatial resolution of  $\Delta x = 0.125^\circ$ , in the range of years 1979–2014.

In all cases, the spatial variance of the fields is defined as:

$$\sigma_\psi = \sqrt{\frac{1}{N} \sum_{l=1}^N (\psi(\mathbf{x}_l, t) - \bar{\psi}(t))^2}, \quad (3)$$

where  $\bar{\psi}(t) = \frac{1}{N} \sum_{l=1}^N \psi(\mathbf{x}_l, t)$  is the average over the system nodes, at positions  $\mathbf{x}_l$ ,  $l = 1, \dots, N$ . This quantity, further

averaged over time, is displayed in Fig. 1b for the LE model.

To construct functional networks from the time series of the LE and GL models at each location  $\mathbf{x}_l$ ,  $l = 1, \dots, N$ , we take  $T = 1000$  temporal snapshots in the asymptotic state  $\{\psi(\mathbf{x}_l, t_k)\}_{k=1, \dots, T}$  (to improve statistics we take them sufficiently distant in time as to be nearly uncorrelated temporally) and compute the Pearson correlation:

$$\rho_{ab} = \frac{\sum_k p_a(t_k)p_b(t_k)}{\sqrt{(\sum_k p_a(t_k)^2)(\sum_k p_b(t_k)^2)}}, \quad (4)$$

where  $p_l(t_k) \equiv \psi(\mathbf{x}_l, t_k) - \frac{1}{T} \sum_k \psi(\mathbf{x}_l, t_k)$ . The network keeps links between pairs of nodes  $(a, b)$  for which  $\rho_{ab} > \gamma$ . For the sea temperature time-series daily functional networks at day  $t$  were built from these time series computing the Pearson correlation with a time window of  $T = 200$  days (100 days before and 100 days after time  $t$ ). The quantities plotted in Fig. 3 are further averaged over 5 days.

To study percolation in these functional networks, as the control parameter  $p$  approaches transition points  $p_d$ , we have measured a number of quantities, namely[11, 12]: a)  $S_1$ , the relative size of the largest connected compo-

ment, i.e. the fraction of nodes that are in the largest cluster. It abruptly changes from a value close to 0 to a value close to 1 at the percolation point. b) The fraction of nodes belonging to clusters of size  $s$ ,  $c_s = sn_s/N$ , where  $n_s$  is the number of clusters of size  $s$  present in the system. This gives also the probability that a randomly chosen node pertains to a cluster of size  $s$ . c) The average size of the clusters excluding the largest one, calculated as  $\sum' sc_s = \frac{1}{N} \sum' s^2 n_s \equiv \langle s^2 \rangle$ , where the sum is over all cluster sizes excluding the largest one. This quantity is maximal at the percolation point.

## Acknowledgements

V.R.-M. was supported by the European Commission Marie-Curie ITN program (FP7-320 PEOPLE-2011-ITN) through the LINC project (Grant no. 289447). We also acknowledge support from FEDER and MINECO (Spain) through the project INTENSE@COSYP (FIS2012-30634) and from the European Commission through project LASAGNE (FP7-ICT-318132).

---

[1] Scheffer, M., Carpenter, S., Foley, J. A., Folke, C. & Walker, B. Catastrophic shifts in ecosystems. *Nature* **413**, 591–596 (2001).

[2] Dobson, I., Carreras, B. A., Lynch, V. E. & Newman, D. E. Complex systems analysis of series of blackouts: Cascading failure, critical points, and self-organization. *Chaos* **17**, 026103 (2007).

[3] van de Leemput, I. a. *et al.* Critical slowing down as early warning for the onset and termination of depression. *Proc. Natl. Acad. Sci. USA* **111**, 87–92 (2014).

[4] Dakos, V. *et al.* Slowing down as an early warning signal for abrupt climate change. *Proc. Natl. Acad. Sci. USA* **105**, 14308–14312 (2008).

[5] Thompson, J. M. T. & Sieber, J. Predicting Climate Tipping As a Noisy Bifurcation: a Review. *International Journal of Bifurcation and Chaos* **21**, 399–423 (2011).

[6] Lenton, T. M., Livina, V. N., Dakos, V., van Nes, E. H. & Scheffer, M. Early warning of climate tipping points from critical slowing down: comparing methods to improve robustness. *Philosophical Transactions of the Royal Society A* **370**, 1185–1204 (2012).

[7] Tsionis, A. A. & Roeber, P. J. The architecture of the climate network. *Physica A* **333**, 497–504 (2004).

[8] Eguíluz, V. M., Chialvo, D. R., Cecchi, G. A., Baliki, M. & Apkarian, A. V. Scale-free brain functional networks. *Phys. Rev. Lett.* **94**, 1–4 (2005).

[9] Timme, M. & Casadiego, J. Revealing networks from dynamics: an introduction. *Journal of Physics A* **47**, 343001 (2014).

[10] Zhou, D., Gozolchiani, A., Ashkenazy, Y. & Havlin, S. Teleconnection Paths via Climate Network Direct Link Detection. *Phys. Rev. Lett.* **115**, 268501 (2015).

[11] Stauffer, D. & Aharony, A. *Introduction to Percolation Theory* (Taylor & Francis Inc, Philadelphia (1994)).

[12] Newman, M. *Networks: An Introduction* (Oxford University Press, Oxford, UK, 2010).

[13] Scheffer, M. *et al.* Anticipating Critical Transitions. *Science* **338**, 344–348 (2012).

[14] Wang, R. *et al.* Flickering gives early warning signals of a critical transition to a eutrophic lake state. *Nature* **492**, 419–22 (2012).

[15] Dakos, V., Carpenter, S. R., Nes, E. H. V. & Scheffer, M. Resilience indicators: prospects and limitations for early warnings of regime shifts. *Philosophical Transactions of the Royal Society of London B* **370**, 20130263 (2015).

[16] Veraart, A. J. *et al.* Recovery rates reflect distance to a tipping point in a living system. *Nature* **481**, 357–359 (2012).

[17] Quail, T., Shrier, A. & Glass, L. Predicting the onset of period-doubling bifurcations in noisy cardiac systems. *Proc. Natl. Acad. Sci. USA* **112**, 9358–9363 (2015).

[18] Scheffer, M. *et al.* Early-warning signals for critical transitions. *Nature* **461**, 53–59 (2009).

[19] Guttal, V. & Jayaprakash, C. Spatial variance and spatial skewness: leading indicators of regime shifts in spatial ecological systems. *Theoretical Ecology* **2**, 3–12 (2009).

[20] Dakos, V., van Nes, E. H., Donangelo, R., Fort, H. & Scheffer, M. Spatial correlation as leading indicator of catastrophic shifts. *Theoretical Ecology* **3**, 163–174 (2010).

[21] Dakos, V., Kéfi, S., Rietkerk, M., van Nes, E. H. & Scheffer, M. Slowing down in spatially patterned ecosystems at the brink of collapse. *The American Naturalist* **177**, E153–E166 (2011).

[22] Van Der Mheen, M. *et al.* Interaction network based early warning indicators for the Atlantic MOC collapse. *Geophysical Research Letters* **40**, 2714–2719 (2013).

- [23] Tirabassi, G. *et al.* Interaction network based early-warning indicators of vegetation transitions. *Ecological Complexity* **19**, 148–157 (2014).
- [24] Feng, Q., Viebahn, J. P. & Dijkstra, H. A. Deep ocean early warning signals of an atlantic MOC collapse. *Geophysical Research Letters* **41**, 6008–6014 (2014).
- [25] Ludescher, J. *et al.* Improved El Niño forecasting by cooperativity detection. *Proc. Natl. Acad. Sci. USA* **110**, 11742–11745 (2013).
- [26] Sarachik, E. S. & Cane, M. A. *The El Niño-Southern Oscillation Phenomenon* (Cambridge University Press, Cambridge, UK, 2010).
- [27] Dijkstra, H. A. The ENSO phenomenon: theory and mechanisms. *Advances in Geosciences* **6**, 3–15 (2006).
- [28] Carpenter, S. R., Ludwig, D. & Brock, W. A. Management of eutrophication for lakes subject to potentially irreversible change. *Ecological Applications* **9**, 75–771 (1999).
- [29] Hohenberg, P. C. & Halperin, B. I. Theory of dynamic critical phenomena. *Rev. Mod. Phys.* **49**, 435–479 (1977).
- [30] ECMWF. European Centre for Medium-Range Weather Forecasts, 2009: ERA-Interim Project [Available online at <http://apps.ecmwf.int/datasets/data/interim-full-daily>].

## Supplementary Information

This Supplementary Information gives additional data on percolation precursors for two different dynamical systems. First, dynamical and percolation transitions are studied for a system displaying regular and chaotic dynamics, the Lorenz'96 model. Second, the behavior with changing threshold is analyzed for the continuous transition experienced by the Ginzburg-Landau model already presented in the main text.

### 1. Transitions and percolation in the Lorenz'96 model

Coupled chaotic oscillators display a large variety of dynamical regimes. Thus, due to the different bifurcations present in those models, they are an excellent test bed to prove the generality of the network-based percolation precursors methodology. Here we consider the Lorenz'96 model [1]. It was proposed by E. Lorenz as a simplified framework to investigate atmospheric predictability. It reads:

$$\frac{d\psi_k(t)}{dt} = [\psi_{k+1}(t) - \psi_{k-2}(t)] \psi_{k-1}(t) - \psi_k(t) + \eta_k(t) + p . \quad (\text{S1})$$

$\psi_k(t)$  is meant to represent the values of some atmospheric variable at different locations  $k$ ,  $k = 1 \dots N$ , arranged in a onedimensional ring around the globe (an thus having periodic boundary conditions). The structure of Eq. (S1) contains some of the main elements of fluid dynamics, namely dissipation, external forcing, and quadratic non-linearity through an advection-like term. In addition to the constant forcing  $p$ , which will be our control parameter, we include an additive stochastic perturbation  $\eta_k(t)$  uncorrelated in space and time. It is implemented here by adding independent random numbers uniform in  $[-a, a]$  ( $a = 0.1$ ) after each time step ( $dt = 1/64$ ) of a fourth-order Runge-Kutta method which is used to integrate the rest of the terms. We focus in the behavior for  $N = 2500$  elements or oscillators. In the absence of the random forcing, three dynamical regimes are easily identified [2]: i) For small  $p$ ,  $p < p_1 = 8/9$ , the system stabilizes in the homogeneous fixed point  $\psi_k(t) = p, \forall k, t$ . ii) for intermediate values of  $p$ ,  $8/9 < p < 4.1$  the system experiences a Hopf bifurcation leading to traveling waves. iii) Beyond  $p > p_2 \approx 4.1$  the system becomes spatiotemporally chaotic.

To display the bifurcations observed when integrating Eq. (S1) for  $N = 2500$  elements we have calculated a Poincare's transversal section in the subspace of two contiguous oscillators: one of the oscillators, say  $\psi_1$ , is monitored and when it crosses the value  $\psi_1 = 1$  in the increasing direction the value of the contiguous oscillator, say  $\phi = \psi_2$  is recorded and displayed. The bifurcation diagram showing the values of these sections  $\phi$  is plotted in figure S1a as a function of  $p$ . The three regimes described above for the deterministic system are readily identified here also.

Functional networks were constructed by interpreting the locations  $k$  as nodes and assigning links between pairs of nodes when the Pearson correlation is larger than a threshold  $\gamma$ . Panel b shows the quantities  $S_1$ , the size of the largest cluster, and  $\langle s^2 \rangle$ , the mean cluster size excluding the largest one, for such network when  $\gamma = 0.16$ . Panels c and d display the properties of several  $c_s$ , the probabilities of randomly chosen nodes to pertain to clusters of size  $s$ . These figures clearly identify the presence of a percolated phase at intermediate values of  $p$ , started and ended by two percolation transitions. Figure S2 shows the quantity  $c_2$  in the  $(\gamma, p)$  parameter plane for this model. We see that for increasing threshold the maxima of  $c_2$  approach the locations  $p_1$  and  $p_2$  at which traveling waves are born at a Hopf bifurcation and give rise to chaotic behavior, respectively. Thus, the percolating phase is a manifestation of the long-range coherence of the traveling wave state, whereas correlation length remains small in the homogeneous and in the chaotic regime. The quantity  $c_2$  (and indeed the other  $c_s$ ) clearly anticipates the first bifurcation when increasing  $p$ . It also largely anticipates the occurrence of a chaos-order transition when decreasing  $p$  from large values.

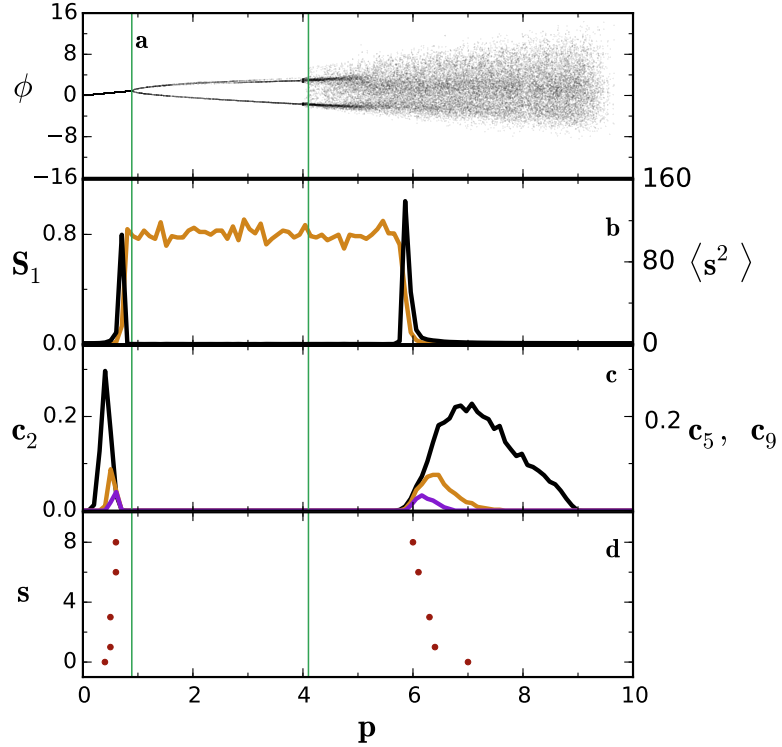


FIG. S1: Panel a shows the bifurcation diagram of the Lorenz'96 model, Eq. (S1), constructed from a 2-oscillator Poincaré section (see text). The transition to traveling waves at  $p_1 = 8/9$  and to spatiotemporal chaos ( $p_2 \approx 4.1$ ) are shown as vertical green lines. Functional networks were built using a threshold of  $\gamma = 0.16$ . The percolation indicators  $S_1$  (orange) and  $\langle s^2 \rangle$  (black) are displayed in panel b. Panel c shows  $c_2$  (black),  $c_5$  (orange), and  $c_9$  (purple). In d, the circles indicate the value of  $p, p_s$  with  $s = 2, 5, 9, 16$  and 21, for which the  $c_s$  curves attain their respective maxima. These indicators reveal a phase of percolated correlations in a parameter region which includes the interval  $[p_1, p_2]$ , flanked by two percolation transitions. The curves have been further averaged over 100 realizations of the random noise and initial condition.

## 2. Changing the threshold in the Ginzburg-Landau model

In the main text (Eq. (2) there) we presented the Ginzburg-Landau model, which experiences a continuous pitchfork bifurcation at  $p = 0$ , and showed the percolation behavior of the functional network constructed at a fixed value of the threshold  $\gamma$ , namely  $\gamma = 0.25$ . Here, we study what happens to the percolation transition when building the networks for different thresholds  $\gamma$ . Figure S3 shows the maxima of  $\langle s^2 \rangle$  (which locate the percolation transitions) and the values of  $c_2$ , in the  $(\gamma, p)$  parameter space. We see that, when increasing  $p$ , the maximum in the precursor  $c_2$  anticipates the percolation transition, which itself anticipates the pitchfork bifurcation at  $p = 0$ . At the other side of the transition, when decreasing  $p$  from the high  $p$  state, the maximum in  $c_2$  also occurs before the percolation transition, which also anticipates the dynamical transition. As in the other models studied the amount of anticipation is larger for lower  $\gamma$ .

---

[1] E.N. Lorenz (1996), *Predictability: A problem partly solved*. in Proc. Seminar on Predictability Vol. I, ECMWF Seminar, edited by T. Palmer (ECMWF, Reading, UK), pp. 1–18.  
[2] A. Karimi and M. R. Paul (2010), *Extensive chaos in the Lorenz-96 model*, Chaos **20**, 043105.

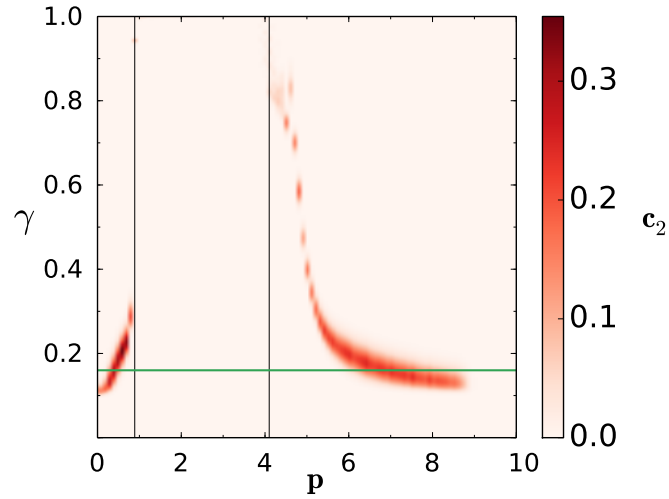


FIG. S2: The  $c_2$  values, as given by the color bar, as a function of the control parameter  $p$  and the threshold  $\gamma$  used to build the functional network for the Lorenz'96 system. The dynamical transitions to traveling waves and to chaos are indicated by the vertical black lines. The horizontal green line identifies the value  $\gamma = 0.16$  for which Fig. S1 was constructed

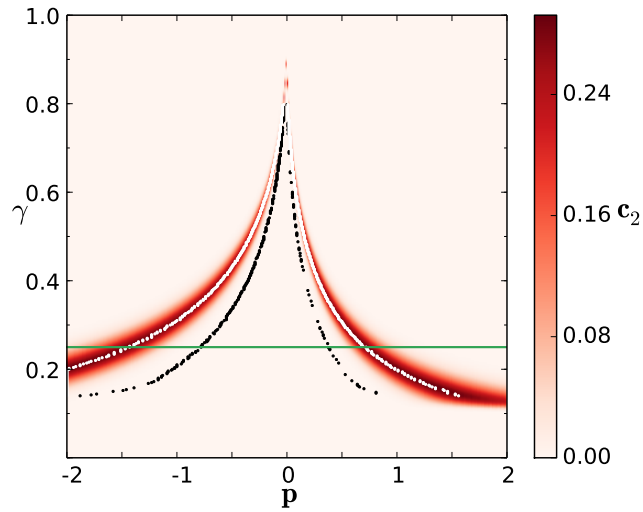


FIG. S3: The  $c_2$  values, as given by the color bar as a function of the control parameter  $p$  and the threshold  $\gamma$  used to build the functional network for the Ginzburg-Landau system. The continuous pitchfork bifurcation occurs at  $p_d = 0$ . Black dots indicate the maxima of  $\langle s^2 \rangle$ , which locate the percolation transition. White dots locate the maxima of  $c_2$ . We see how the percolation transition and its precursor  $c_2$  anticipate in different amounts (when increasing  $p$  from the low  $p$  state, or when decreasing  $p$  from the high  $p$  state) the dynamical bifurcation. The horizontal green line identifies the value  $\gamma = 0.25$  for which Fig. 2 of the main text was constructed.